Marine Geology 336 (2013) 160–169

Contents lists available at SciVerse ScienceDirect

Marine Geology

journal homepage: www.elsevier.com/locate/margeo

Sediment dynamics during Heinrich event H1 inferred from grain size

Laura deGelleke [a,*], Paul S. Hill [a], Markus Kienast [a], David J.W. Piper [b]

[a] Department of Oceanography, Dalhousie University, 1355 Oxford Street, PO Box 15000, Halifax, NS, B3H 4R2, Canada
[b] Geological Survey of Canada (Atlantic), Bedford Institute of Oceanography, PO Box 1006, Dartmouth, NS, B2Y 4A2, Canada

ARTICLE INFO

Article history:
Received 10 November 2011
Received in revised form 26 December 2012
Accepted 27 December 2012
Available online 10 January 2013

Communicated by J.T. Wells

Keywords:
sediment transport
Heinrich event
H1
DIGS
entropy analysis

ABSTRACT

Throughout the last glacial period, massive volumes of icebergs were discharged periodically through Hudson Strait during so-called Heinrich (H) events. These icebergs transported sediments that were subsequently deposited in distinct layers across the North Atlantic as they melted. The objective of this research was to measure and describe sedimentation associated with a meltwater plume discharged during the H1 ice-rafting event at about 17 ka by examining sediment texture. The H1 layer was sampled in 11 piston cores that cover about 4000 km of the slope between Hudson Strait and the Gulf of Maine. Disaggregated inorganic grain size (DIGS) distributions were determined using a Coulter Counter. Additionally, the $CaCO_3$ content and the >63 μm fraction were measured and DIGS distributions were sorted using entropy analysis. Entropy analysis proved to be a useful tool for distinguishing between sediment delivery mechanisms. Textural interpretation of sediment dynamics during the H1 event was broadly consistent with facies interpretations. H1 layer sediments were mainly delivered by plume and ice-rafting, with some samples showing higher-energy sorting. In general, plume deposition was dominant within 1000 km of Hudson Strait, and distal sediments were mainly delivered by ice-rafting. Entropy analysis of DIGS distributions provides a robust means of understanding fine fraction (<100 μm) sediment dynamics in H events.

1. Introduction

Throughout the last glacial period, massive volumes of icebergs were discharged periodically from the Hudson Strait region during so-called Heinrich (H) events (Broecker et al., 1992). These icebergs transported sediments that were deposited in distinct layers across the North Atlantic as they melted. Hemming (2004) estimated a total discharge of 3×10^4 km^3 to greater than 5×10^6 km^3 of ice was required to account for the sediment deposited across the deep North Atlantic ocean. The occurrence of H events has been correlated with cold events recorded in Greenland ice cores (Bond et al., 1993; Dansgaard et al., 1993; Broecker, 1994). Millennial-scale variability in Antarctic ice cores, marine sediment cores, lake sediments, and cave stalagmites also correlates with variability observed in Greenland ice cores (Voekler, 2001). The abrupt nature of the variability and the correlation of global records suggest that the occurrence of H events is intimately linked to the global ocean–atmosphere system.

In the North Atlantic deep-sea sediment cores, H layers were first identified from a sudden increase in coarse-grained detrital carbonate (DC) and lithic fragments termed ice-rafted detritus (IRD) and from a reduced concentration of foraminifera (Heinrich, 1988). In the northwest Labrador Sea, correlative DC layers are equivalent to H layers in the North Atlantic (Andrews and Tedesco, 1992), but include sediment delivered by other ice-proximal transport processes that result in a somewhat different anatomy (Rashid et al., 2003a). Here, both North Atlantic H layers and Labrador Sea DC layers are referred to as H layers. H layers near the Hudson Strait are enriched in fine-grained DC at concentrations that could not have been delivered by ice-rafting alone and suggest delivery by a meltwater plume (Hesse and Khodabakhsh, 1998). Research on H events has largely been focused on timing, duration and provenance, with the assumption that the significant mechanism of sediment transport was iceberg rafting (Andrews, 1998). However, considerable evidence indicates that depositional and transport processes are much more complicated in ice-proximal regions where debris flows and turbidites are common (Andrews et al., 1994; Wang and Hesse, 1996). The character of sediments deposited proximally in the Labrador Sea indicates that H ice-rafting events were accompanied by massive meltwater discharge, rich in carbonate sediments (e.g., Hillaire-Marcel et al., 1994; Hesse and Khodabakhsh, 1998; Rashid et al., 2003b). However, little attention has been given to understanding the sedimentation associated with this meltwater discharge.

Icebergs and meltwater discharged during H events are advected great distances with the prevailing currents and have significantly affected the hydrology of the region. Distinct H layers have been identified in the Labrador Sea (Andrews and Tedesco, 1992) and across the North Atlantic (e.g., Bond et al., 1992; Grousset et al., 1993; Dowdeswell et al., 1995) as far as the Iberian margin (e.g., Lebreiro et al., 1996; Bard et al., 2000). Evidence from foraminifera indicates that low temperature and low salinity surface waters extended much farther south during H events (Bond et al., 1992; Hillaire-Marcel et al.,

* Corresponding author. Tel.: +1 902 293 8635.
E-mail address: laura.degelleke@dal.ca (L. deGelleke).

0025-3227/$ – see front matter © 2013 Elsevier B.V. All rights reserved.
http://dx.doi.org/10.1016/j.margeo.2012.12.007

1994). Multiple proxies have been used to suggest that hydrological changes in surface waters across the North Atlantic during H events caused a reduction of North Atlantic Deep Water (NADW) formation (Keigwin and Lehman, 1994; McManus et al., 2004) and models have demonstrated this possibility (Stocker, 2000; Khodri et al., 2003). Investigating sediment transport during H events will help constrain the discharge and better our understanding of these significant climate events.

This work aims to build an understanding of the meltwater component of the H1 ice-rafting event that occurred at about 17 ka by investigating the sediment texture of H1 layers in marine sediment cores from the Labrador, Grand Banks, and Scotian slopes. Specifically, the fine (<100 μm) disaggregated inorganic grain size (DIGS) distributions in H1 layers are examined across the region in an attempt to identify sediment delivery mechanisms.

2. Geological and oceanographic setting

The eastern Canadian continental shelf (Fig. 1) has been shaped by Pleistocene glaciations that resulted in numerous transverse troughs and intervening banks (Piper, 1988). The mean depth of the continental shelf and shelf break decreases from north to south. Near Hudson Strait, the shelf break occurs at about 500 m while the break occurs at about 100 m in places off the Scotian Shelf and Grand Banks. Large areas of the Scotian Shelf and Grand Banks are less than 100 m deep and would have been emergent during glacial lowstands (Piper, 2005). The depth of the ocean basin itself increases from 2200 m in Baffin Bay, to 3000–4000 m in the Labrador Sea, to over 5500 m in the central North Atlantic Ocean.

The Labrador Current is a strong western boundary current that flows southward along the shelf break in the Labrador Sea and continues around the Grand Banks and along the Scotian Slope, typically winnowing the seabed down to 1500 m (Talley and McCartney, 1982). The cold Labrador Current meets the warmer Gulf Stream near the Grand Banks leading to complicated circulation patterns. Much less is known about the past circulation of the North Atlantic. While it is reasonable to expect some differences in past circulation, the ocean basin shape, wind forcing, and Coriolis forcing that result in the current general circulation pattern are not expected to have been significantly different during the H1 event. Meltwater and icebergs discharged from the Hudson Strait region during the event would have been advected south in a surface plume along the shelf edge in the Labrador Current. At Orphan Basin, some discharge would be advected eastward across the ocean in the North Atlantic Current while some would continue south through Flemish Pass, around the Tail of Grand Banks, and along the Scotian Slope.

3. Methods

The total thickness of the H1 layer was recorded in 104 piston cores and along-margin distance from the mouth of Hudson Strait was estimated (±100 km) to represent the distance that any plume would have traveled to the core location with the prevailing current.

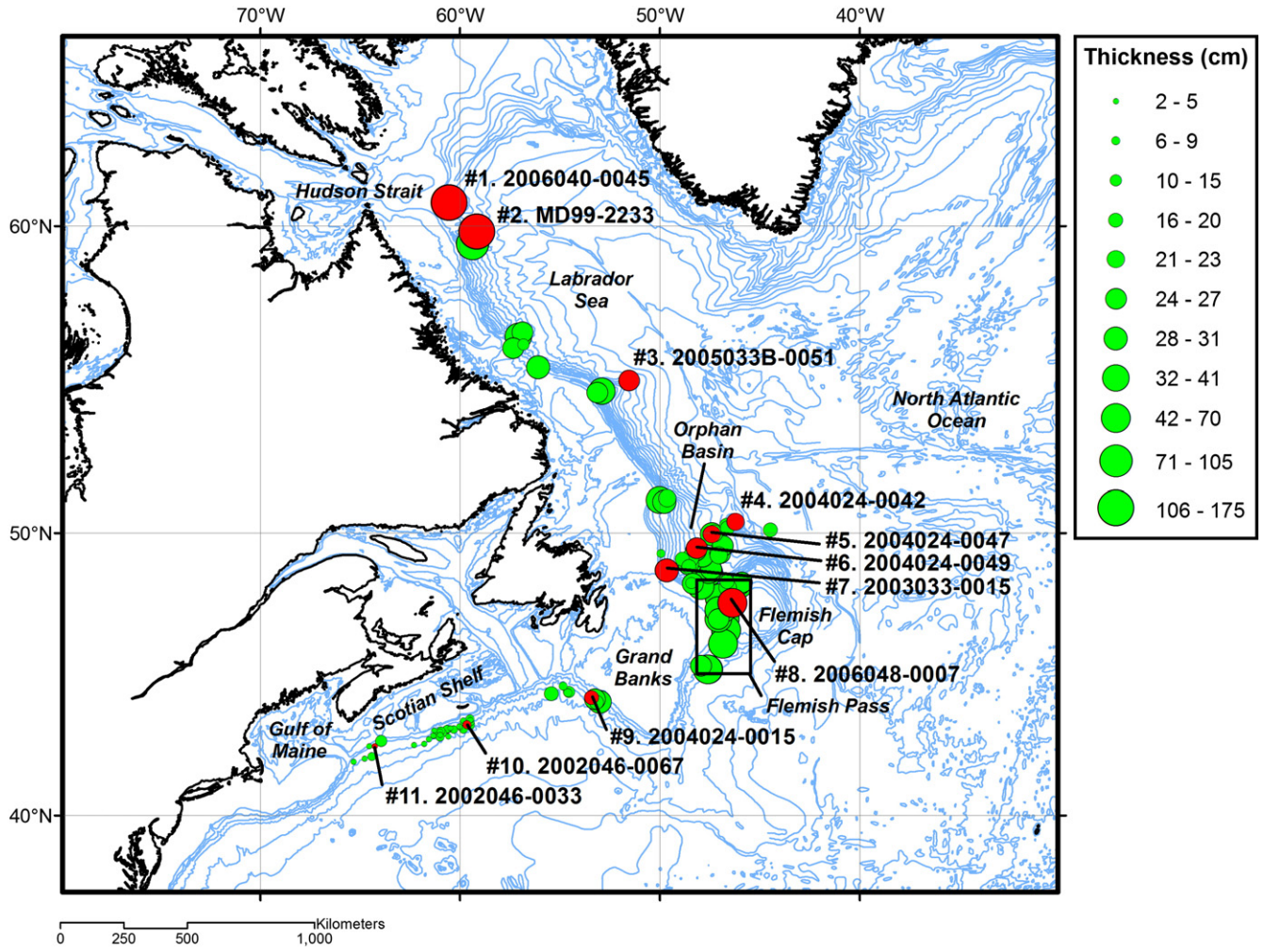

Fig. 1. H1 layer thicknesses (cm) in 104 cores from the western North Atlantic. The size of the core location marker indicates layer thickness. The location of eleven cores chosen for grain size analysis and determination of calcium carbonate and sand & gravel content is highlighted. Two transects are available to investigate variability: a proximal to distal along-margin transect of eight cores (1–3, 5, and 8–11) and a cross-margin transect of four cores (4–7) in Orphan Basin.

Typically, the H1 layer was defined by carbonate content, most often indirectly from visual or instrumental detection of lightness but also directly from calcite and/or dolomite measurements. Because of the inaccuracies arising from bioturbation, these thicknesses have an estimated error of 1–10% associated with them.

Eleven cores with H1 layers were selected for grain size analysis (Fig. 1). These cores cover approximately 4000 km of the margin between Hudson Strait and the Gulf of Maine and range in water depth from 818 to 2740 m. Except for core 1, core locations avoid sites immediately seaward of transverse troughs, where there is potential for the greatest local meltwater supply. Core locations allow construction of a proximal to distal along-margin transect of eight cores as well as a cross-margin transect of four cores in Orphan Basin.

Core photography and X-radiographs were used to identify the H1 layer in each core. This is possible because high carbonate content in H1 layers of this region results in sediment much lighter in color and denser than the background sediment. Each layer was subsampled at regular intervals. Vertical spacing of subsamples taken from each core varied because of the different H1 layer thicknesses and inter-sample spacing ranges from 2–11 cm. The thicker H1 layers in cores from the Labrador slope and Grand Banks region were sampled at larger intervals, and the thinner H1 layers in cores from the Scotian margin were subsampled at smaller intervals. At least one sample above and one sample below the H1 layer were analyzed to characterize background sediment texture. A total of 154 samples were taken, and the number of samples per core ranged from 6 to 18.

The disaggregated inorganic grain size (DIGS) of each sample was determined with a Beckman Coulter Counter Multi-sizer III (MS3) using a procedure similar to that described in Milligan and Kranck (1991). Use of the Coulter Counter for determining grain size was favored over the Sedi-graph because of the accommodation of small sample sizes and the importance of characterizing the fine tail of the size distribution precisely (see McCave and Hall (2006) for more on particle size analysis instruments). In preparation for analysis, samples were dried in an oven at 40 °C and organic matter was digested with 30% H_2O_2 solution that was subsequently evaporated from the sample on a hot plate. Digested samples were resuspended in 0.45 μm filtered 1% NaCl and sonified using a sapphire-tipped ultrasonic probe immediately before analysis to disaggregate component grains. Samples were run using two tubes with aperture sizes of 30 and 200 μm, which were able to resolve particle of diameters 0.6–100 μm. To prevent large grains from clogging the aperture, sample solutions were screened at 100 μm prior to analysis with the 200 μm tube and then at 25 μm prior to analysis with the 30 μm tube. The MS3 outputs particle counts for each tube in 256 bins in 1/50ϕ increments. Using a Matlab routine, the particle counts were summed across 10 bins and re-binned in 1/5ϕ increments using the midpoint diameter. Bins with counts below 10 were discarded and each tube distribution was normalized to produce a single distribution curve for each sample.

Reproducibility of the grain size distributions measured by the MS3 was gauged using a poorly-sorted glacial sediment collected in Sillikers, New Brunswick. This sediment serves as a standard to gauge instrument precision and to assess instrument performance. It is referred to simply as "Sillikers". A total of 14 Sillikers subsamples were run on the MS3 and a mean distribution with a modal diameter of 10.56 μm was calculated with standard deviation minimum of 0.11 vol.%, maximum of 0.39 vol.%, and median of 0.24 vol.%. Because Sillikers subsamples are taken from a sample orders of magnitude larger than the core samples analyzed here, Sillikers subsamples are expected to contain more variability and represent the lower limit of reproducibility for the MS3.

Prior to digestion, a portion of each dried sample was ground with a mortar and pestle, weighed, and analyzed for total inorganic carbon content using a UIC Inc. CM5130 acidification module and CM5014 coulometer. 2 N H_2SO_4 was added to ~20 mg of sample and heated in the acidification unit. The liberated CO_2 was carried into the coulometric cell where it reacted to form a titratable acid. Calcium carbonate ($CaCO_3$) content was calculated using total inorganic carbon mass and assuming no other carbonate-bearing species was present. Calcite is the dominant carbonate mineral in H layer sediments in the Hudson Strait region and is generally found to be more than twice as abundant as dolomite during H events (Andrews et al., 1994). Two complications arise from the possible presence of dolomite. First, dolomite is more resistant to acid dissolution so its carbon may not have evolved and been measured by the coulometer. Second, dolomite contains two carbonate groups and would produce twice as much carbon as calcite for each dissolved molecule. Although the effect of dolomite on the carbonate measurements is uncertain, the error would be systematic so relative comparisons can be made. Analytical precision and accuracy were calculated each time the instrument was run using pure $CaCO_3$ and NRC MESS-3 marine sediment standards and were found to be less than $\pm 1.0\%$ and $\pm 1.8\%$ respectively.

A portion of each digested sample was suspended in a filtered 1% NaCl solution and divided into a fine (<63 μm) and coarse (>63 μm) fraction by screening. Both fractions were filtered through a preweighed millipore 8.0 μm filter under vacuum. The use of this size filter is recommended in previous studies (e.g., Sheldon et al., 1972; Law et al., 2008), because it has much smaller nominal pore sizes once filtering begins but is not as prone to clogging. The filters and collected grains were dried and weighed and then used to calculate % sand & gravel for each sample. In an open-ocean setting, % sand & gravel would be equivalent to % IRD since ice-rafting is the dominant process that can account for delivery of coarse grains to the seafloor. Dust observed in pelagic sediments are rarely (<5%) greater than 6–8 μm and typical dust sedimentation rates are negligible compared to the rapid sedimentation rates during the H1 (Rea, 1994). However, in a slope setting, turbidity currents also deliver a significant portion of coarse grains to the seafloor. Thus, % sand & gravel in these samples represents the portion of the sample not delivered by plume but by ice-rafting and/or turbidity currents.

4. Entropy analysis

Entropy analysis was used to investigate DIGS distribution variability. In information theory, entropy is a measure of the randomness associated with a variable and was first described by Shannon (1948). In essence, entropy describes the information content, since the value of a measured variable decreases with increasing randomness. Applied to particle size distributions, entropy is greatest and randomness is at a maximum when particles are evenly distributed between all size classes (i.e. poorly-sorted). On the other hand, entropy is least and there is no randomness in a distribution when all particles are found in one size class (i.e. well-sorted). In this way, entropy can be used to describe particle size distributions. Because the entire size distribution is taken into consideration, entropy analysis provides insight not available through more traditional particle size distribution descriptors such as mean particle diameter and standard deviation.

The concept of entropy has been successfully applied to interpretation of sediment size distributions. Johnston and Semple (1983) used a FORTRAN routine to apply the information theory of Shannon (1948) to various data sets. This was later adapted to sediment size in a QBASIC routine by Woolfe and Michibayashi (1995), who showed that entropy analysis of bottom sediment size distributions provided groupings that could be correlated to depositional environment. Since, many more researchers have confirmed that entropy groupings can be meaningfully associated with sediment facies. More recently, Orpin and Kostylev (2006) used entropy analysis to characterize bottom sediment texture on the Scotian Shelf and to define ecological habitats, and Mikkelsen et al. (2007) used entropy analysis to investigate the role of turbulence variation on floc formation. An adaptation of the entropy analysis routine of Mikkelsen et al. (2007) was used to group the core sample DIGS distributions in this study. This routine is a Matlab

translation of the QBASIC routine used by Woolfe and Michibayashi (1995). Similar routines have been published (e.g., Stewart et al., 2009).

For a particle size distribution with n size classes, the entropy, E, is given by

$$E = -\sum_{i=1}^{n} p_i log_2 p_i, \quad (1)$$

where p_i is the proportion of particles in size class i (Shannon, 1948; Johnston and Semple, 1983). Entropy can be related to information gain or inequality statistic, I, by $I = \log_2 n - E$. This reflects the concept that as entropy decreases and volume within a distribution is concentrated into fewer size classes, the distribution becomes more informative in regards to particle processes and depositional environment.

Sample DIGS distributions are grouped using the inequality statistic by maximizing the inequality between groups and minimizing the inequality within groups. In order to do this, the volume of particles in each size class in each distribution must be expressed as proportions of the total volume of all size classes in all distributions (Johnston and Semple, 1983). Following Mikkelsen et al. (2007), the proportion of the total volume concentration in a distribution j, size class i is Y_{ij} and is defined as

$$Y_{ij} = \frac{VC_{ij}}{\sum_{j=1}^{J}\sum_{i=1}^{N} VC_{ij}}, \quad (2)$$

where N is the total number of size classes in each distribution, J is the total number of distributions, VC_{ij} is the volume concentration in a distribution j, size class i. The total inequality for all distributions is then given by

$$I = \sum_{i=1}^{N} Y_i \sum_{j=1}^{J} Y_j log_2 N\ Y_j, \quad (3)$$

where $Y_i = \sum_{j=1}^{J} Y_{ij}$ and $Y_j = Y_{ij}/Y_i$.

The percentage of the inequality in the distributions explained by the grouping is the R_s statistic (Johnston and Semple, 1983) whose value is $R_s = (I_B/I) * 100$, where I_B is the inequality between groups defined as

$$I_B = \sum_{i=1}^{N} Y_i \sum_{j=r}^{R} p_{ir} log_2 \left(\frac{p_{ir}}{J_r/J}\right), \quad (4)$$

where $p_{ir} = (\sum_{j \in r} Y_{ij})/Y_i$ and J_r is the number of distributions in group r of R total groups (Mikkelsen et al., 2007). To obtain an optimal grouping defined as the best R_s statistic, it is necessary to perform calculations for all the possible combinations of J into R groups for each R and then use the combination with the greatest R_s. Similarly, to obtain the optimal number of groups, the optimal grouping must be determined for r of R groups then for $r+1$ groups, and the resulting R_s statistics are compared to assess validity of the groupings. The routine ends when increasing the number of groupings fails to increase the R_s statistic. An additional qualitative criterion is typically applied to the selection of number of groups in sedimentological applications (e.g., Orpin et al., 2004), whereby field observations of number of sediment facies are used to select group number. Here, sample DIGS distributions are divided into three groups yielding a R_s value of 66.0%. The optimum number of groups for the distributions was determined to be 13 with a R_s value of 88.3%. However, three groups explain a majority of the variability and provide distinct groups that can be associated with the sediment facies observed in H layers.

5. Results

5.1. H1 layer thickness

The thickness of the H1 layers in 104 cores from the study region ranges from 2–175 cm (Fig. 1). H1 layer thickness decreases exponentially with increasing along-margin distance (Fig. 2). This trend supports a single source of sediment delivery to the Labrador Sea during the H1 event from the Hudson Strait region. Much of the Labrador Slope (700–1000 km) contains cores with H1 layers that are thinner than predicted by the exponential relationship, while the Orphan Basin and Flemish Pass regions (1700–2200 km) contain cores with H1 layers that are generally thicker than predicted. No trend in H1 layer thickness with water depth was apparent at any distance from the Hudson Strait (not shown). However, H1 layers with distinctive DC are absent on the upper Labrador Slope (<700 m) and on the upper Scotian Slope (<1000 m). The lack of a cross-margin trend in thickness negates significant cross-margin transport (i.e., resulting from meltwater discharged at various points along the margin or mass transport events after deposition).

5.2. DIGS entropy analysis

All sample DIGS distributions were divided into three groups using entropy analysis (Fig. 3). Group #1 has the greatest volume of fine grains and the smallest median diameter, group #3 has the greatest volume of coarser grains <100 μm and the largest median diameter, and group #2 has an intermediate median diameter and contains the majority of its volume at these intermediate sizes.

The group assigned to each core sample DIGS distribution is presented downcore in Fig. 4. The number of samples in each core varies from 6 to 18, generally decreasing with distance from the source, and is a good indicator of relative thickness of the H1 layer. Occurrences of group #1 range from 0 to 14 per core. In general, the occurrence of group #1 decreases with distance from the source along-margin and is completely absent in some distal cores. The number of occurrences of group #2 with along-margin distance is between 4 and 12 per core and fairly constant, although the total number of samples per core is decreasing. Occurrences of group #2 increase slightly with along-margin distance until the Flemish Pass region (core 8) where they are highest at 12 occurrences and decrease slightly thereafter. The occurrence of group #3 is sporadic ranging from 0 to 5 occurrences per core and does not show any obvious along-margin evolution. The number of occurrences of group #1 is directly related to layer thickness.

In terms of cross-margin variability, the occurrence of group #1 ranges from 2 to 6 and decreases with seaward distance. Cross-margin occurrences of group #2 range from 8 to 10 per core and group #3 occurrences range from 1 to 4 per core. There is no significant trend in the occurrence of group #2 cross-margin and occurrences of group #3 increase with seaward distance cross-margin, being most abundant on the crest of Orphan Knoll, an offshore bedrock high.

Group #1 comprises the majority in core samples at the start of the H1 event and decreases as the event proceeds while the occurrence of group #3 increases during the event to comprise a significant portion of samples at the end of the event. The occurrence of group #2 samples is fairly constant through the duration of the event.

5.3. Calcium carbonate and sand & gravel content

The median $CaCO_3$ content within the H1 layers decreases from 47 to 13% with distance from the source (Fig. 5). Lowest median % sand & gravel is recorded proximally at 8%. The sand & gravel content initially increases with distance from the source and then decreases, peaking with a median value of 25% in Orphan Basin (core 5) and of 27% off the SW Grand Banks (core 9). Cross-margin, the median % $CaCO_3$ is between 28 and 35% and the median % sand & gravel ranges between

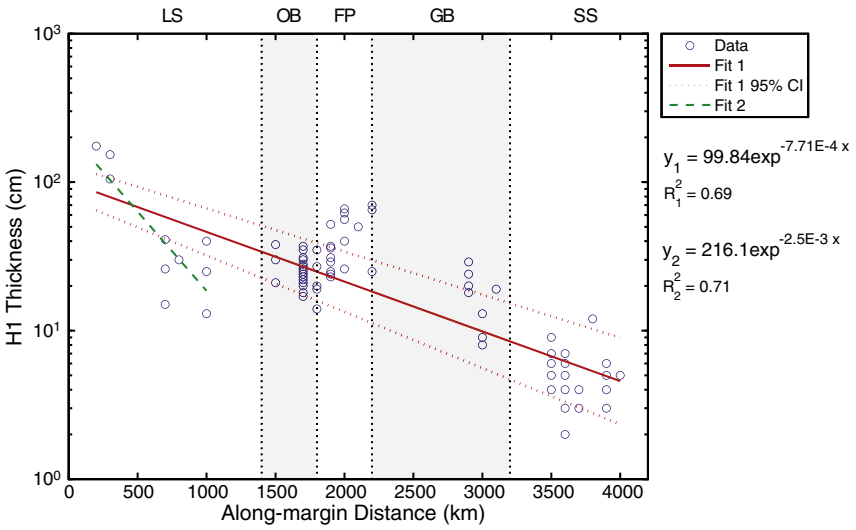

Fig. 2. H1 layer thickness (cm) by along-margin distance (km) on semilog-y axes for 104 cores from the western North Atlantic. Fit 1 is a linear regression of all recorded layer thicknesses and is plotted with 95% confidence intervals. Fit 2 is a linear regression of layer thicknesses in cores only within 1000 km of Hudson Strait. The equations and R^2 values for both fits are shown. Regions discussed are shaded in the figure background. LS = Labrador Slope, OB = Orphan Basin, FP = Flemish Pass, GB = Grand Banks, SS = Scotian Slope.

21% and 27% (Fig. 6). Both % $CaCO_3$ and % sand & gravel have smaller ranges of values cross-margin than along-margin and both have maxima at core 6. Core 7 is a particularly shallow core (818 m) and appears to have the distinctly lower values of both % $CaCO_3$ and sand & gravel in the cross-margin transect.

At the start of the event, the $CaCO_3$ content quickly increases from a median value of 10% to a maximum at 41% (layer fraction 0.2–0.3 bin) (Fig. 7). Then, % $CaCO_3$ slowly decreases for the duration of the event but does not return to pre-H1 levels. The % sand & gravel in the core samples shows a similar trend although less pronounced with medians ranging from 11 to 25%.

6. Discussion

6.1. Association of textural groups with delivery mechanisms

Entropy analysis allowed all DIGS distributions to be divided into three textural groups. Each of these textural groups can be associated with an environment necessary to produce that size distribution in bottom sediments. According to facies analysis (e.g., Rashid et al., 2003b), three main delivery mechanisms are characteristic of the region during H events: plume fallout, ice-rafting, and turbidity currents. In addition, fines may be winnowed out of sediment by the Labrador Current. Especially when bedding is thin, samples may include sediment delivered by more than one mechanism. In this case, entropy analysis identifies only the dominant mechanism.

Because the group #1 average grain size distribution is poorly sorted and has the largest volume-percent of the finest particles, it is most likely to result from flocculated plume-style deposition. Aggregation of grains into flocs is not size-biased and floc deposition removes sediment in the same proportions it is found in suspension (Kranck, 1980). Milligan et al. (2007) measured DIGS in the bottom sediments of the Po River Delta beneath a 100-year-flood plume and found highly flocculated deposits that closely resemble the group #1 spectrum.

The average distribution of group #3 has an abundance of well-sorted coarse particles that would result from higher-energy sorting. Similar distributions have been found in turbidite sequences of cores on the Laurentian Fan (Curran et al., 2004) and turbidity currents are a common high-energy sedimentological process in the region (Piper, 2005). However, turbidity currents cannot deposit carbonate-rich sediment on top of Orphan Knoll (core 4), nor on the lower Scotian Slope (cores 10 and 11), where upslope sediments have extremely low carbonate abundance (Piper and Skene, 1998). Higher abundance of group #3 is associated with lower abundance of carbonate, especially in the upper part of the beds. This could be explained by winnowing of carbonate rich fines from the bed or by dilution of the DC bed by sediment from a different source with a coarser initial size distribution.

Group #2 has the least sorted distribution and contains a significant amount of coarser material. It is most likely associated with sediment delivery by ice-rafting. It is also possible that ice-rafted sediment with a group #2 distribution was deposited and then winnowed to produce a group #3 distribution. In this situation, the removal of fine sediment would result in elevated % sand & gravel. Average sand & gravel content is slightly greater in group #3 distributions (23.8%) than in group #2 ice-rafted distributions (22.6%) suggesting that winnowing of some samples may have occurred (figure not shown).

Modern analogs exist linking group #1 (e.g., Milligan et al., 2007) and group #3 (e.g., Curran et al., 2004) sediment distributions to plume and high-energy sediment transport mechanisms respectively. A logical argument is presented for the association of group #2 distributions with ice-rafting delivery. If the association between the entropy groups and the sediment delivery mechanisms is accepted, the following discussion of the H1 event and conclusions are reasonable.

6.2. The H1 event using sediment texture

By investigating downcore changes in sample entropy group in the context of the associated depositional environment, a reconstruction of the H1 event unfolds and is supported by variability in H1 layer thickness, % $CaCO_3$, and % sand & gravel. Temporally, group #1 dominates sediments deposited at the beginning of the H1 event (Fig. 4). This implies that freshwater discharge was greatest at the beginning of the event and/or the ice margin retreated during the event. Spatially, the occurrence of group #1 is greatest proximally and significantly decreases with distance along the margin. This aligns with the expectation that the rate of plume-style sedimentation should decrease with distance from the source and lends support to Hudson Strait as the major source of meltwater discharge. Additionally, the decreasing cross-margin trend in the occurrence of group #1 suggests that more seaward cores were located beyond the edge of the plume

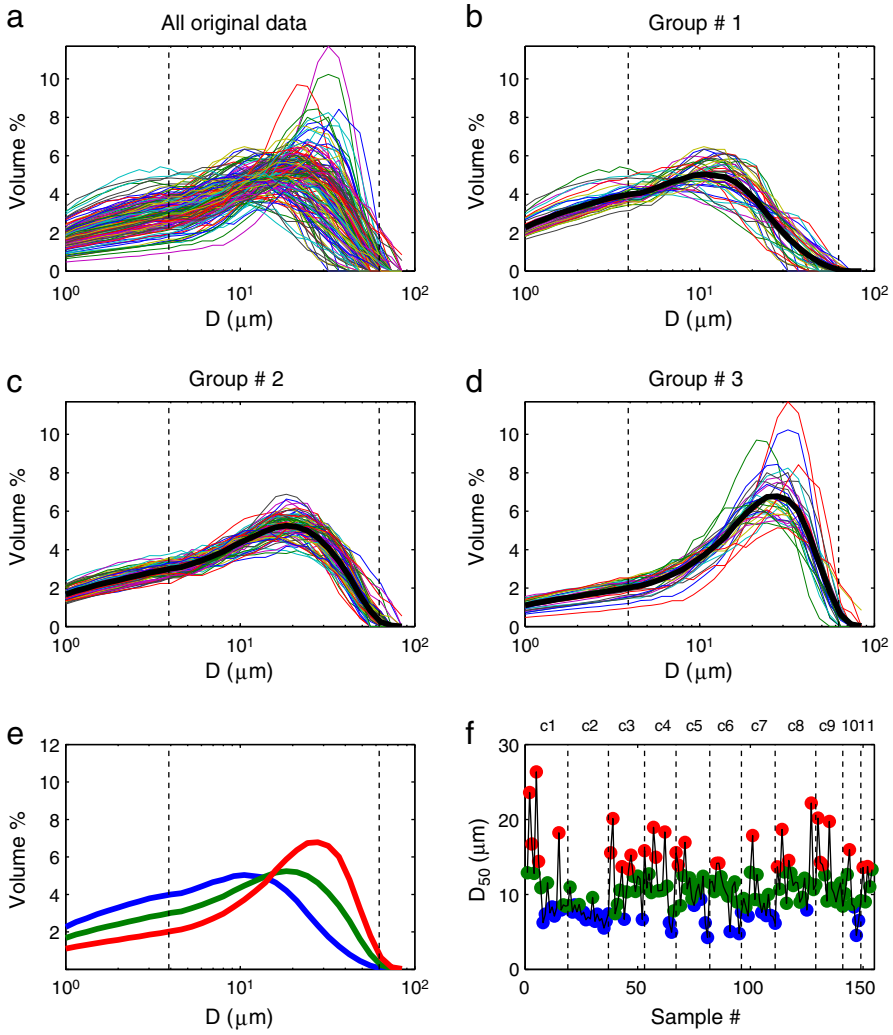

Fig. 3. Entropy analysis of sample DlGS distributions (<100 μm fraction) showing (a) all core sample distributions (b) entropy group #1 distributions with the average group distribution shown in bold (c) entropy group #2 distributions with the average group distribution shown in bold (d) entropy group #3 distributions with the average group distribution shown in bold (e) the average group distribution for all three groups on the same axes (f) the median diameter of each sample distribution colored by group. Axes are semilog-x in (a–e) and standard limits for clay-silt at 3.9 μm and silt-sand at 62.5 μm are shown by dotted vertical lines for reference. In (e) and (f) group #1 is shown in blue, group #2 is shown in green, and group #3 is shown in red. In (f) the sampled cores are labeled on the top x-axis.

trajectory as it moved southward while hugging the slope. In contrast to passive movement of the plume with the slope current, icebergs would also be subject to wind forcing.

To address the feasibility of rapid plume deposition in the proximal region, a calculation can be performed to estimate the distance sediment would be carried by a typical coastal plume before deposition. The *e*-folding distance, x, that particles with a settling velocity, w_s, will travel in a plume of thickness, h, with current speed, u, is $x = h\ u/w_s$. Consider a flocculated plume 100 m thick traveling 50 cm/s with a typical bulk settling velocity of 0.1 mm/s (Hill et al., 2000; Curran et al., 2002). After traveling 500 km, sediment concentrations would have fallen to $1/e$ of their initial concentration, assuming no dilution by mixing. Cores 1 and 2 are both within 500 km of Hudson Strait and are the only cores for which group #1 is abundant.

In Fig. 4, the occurrence of group #2 is relatively constant within cores suggesting that ice-rafting occurred throughout the H1 event and was steadily delivering sediment to the seafloor. Occurrences of group #2 are slightly elevated in Orphan Basin (cores 4–7) and Flemish Pass (core 8). Today, this is a region of complicated circulation where the Labrador Current encounters bathymetric barriers, and much of it is forced through the relatively narrow Flemish Pass. Additionally, it is near this region that the cold, south-flowing Labrador Current begins to mingle with the warmer, north-flowing Gulf Stream as it continues its northeastward path across the North Atlantic Ocean. These conditions could have caused either a slowing of iceberg advection or increased melting rates in the region or a combination of both. Icebergs moving more slowly and/or melting more quickly would have delivered more sediment to the seafloor, explaining the increased occurrence of group #2 in the Orphan Basin and Flemish Pass regions and the proportionally greater thickness of the H1 layer in these regions (Fig. 2).

The occurrence of group #3 is indicative of higher-energy sorting and appears to be sporadic over distance and becomes more abundant over the course of the event as shown in Fig. 4. Turbidity currents can occur when sediment accumulates rapidly on slopes and is subsequently disturbed by physical forcing. Conditions for triggering turbidity currents would vary spatially due to local differences in bathymetry, current, and sediment supply. As a result, turbidites may appear randomly over great areas when these local differences have not been considered. The occurrence of group #3 increases towards the end of the event, when large amounts of sediment previously deposited during the event may have contributed to slope instabilities resulting in turbidity currents. Furthermore, cross-margin variation in cores 5–7 shows an increase in group #3 occurrence downslope and seaward that correlates with where turbidite deposits are expected to

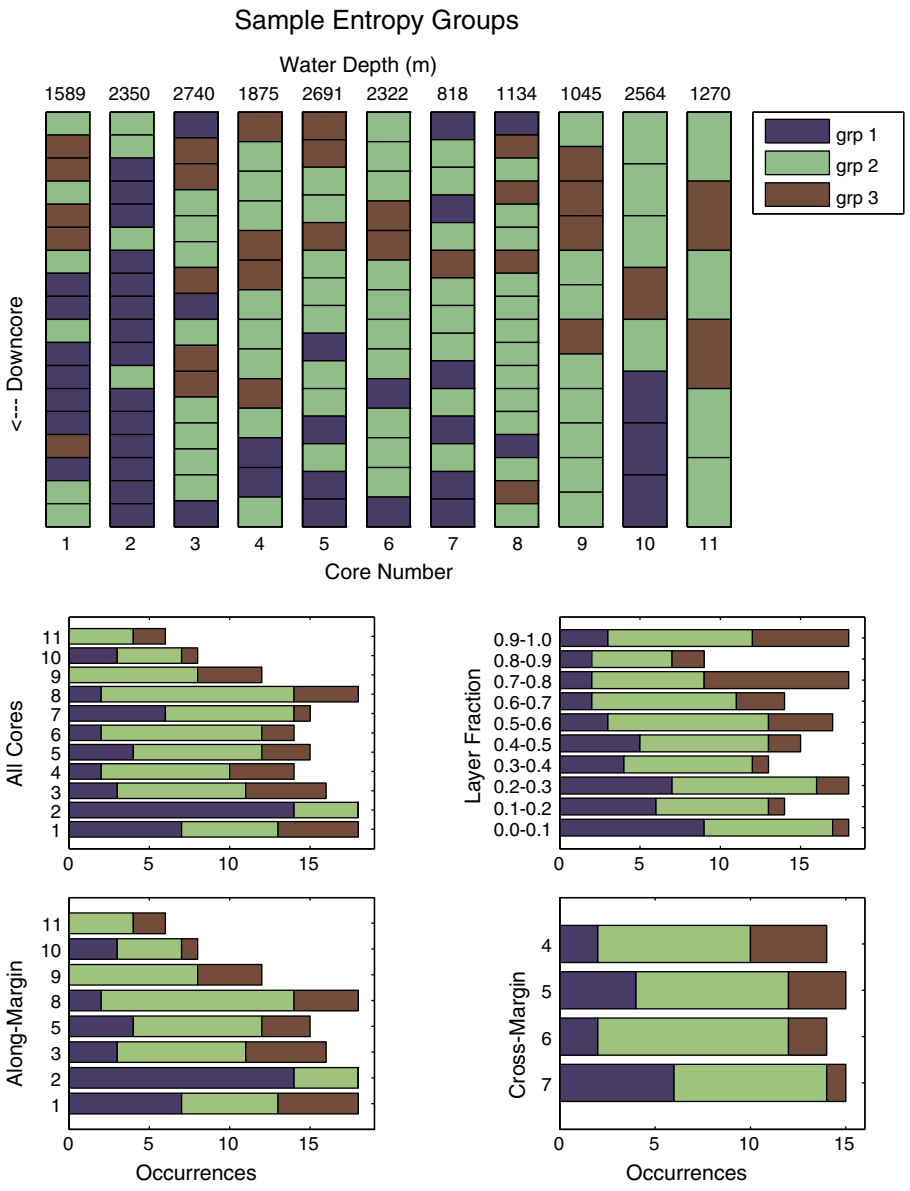

Fig. 4. The entropy group # of each sample DIGS distribution is shown through each core. Cores are presented from left to right in order of increasing along-margin distance. Water depth (m) is listed above each core. Histograms show the number of occurrences of each group in all cores, by layer fraction, by cores in the along-margin transect, and by cores in the cross-margin transect.

be found. Core 4 is located atop Orphan Knoll where occurrences of group #3 distributions are likely a result of winnowing. In proximal cores, Rashid et al. (2003a) demonstrated from X-radiography that DC turbidites were abundant in the uppermost part of H1 in some cores. It is, however, not possible from DIGS data alone to distinguish the relative importance of turbidity current flow or winnowing by the Labrador Current, which would both result in the creation of group #3 sediments.

H1 layer thickness supports the H1 event scenario painted by the entropy groupings. The layer thickness within a particular core is the result of the overall sedimentation rate at that particular location. Based on the entropy groupings, three main sediment delivery mechanisms have been identified. Thus, the layer thickness is a result of the summation of all sedimentation from all three mechanisms during the event. With this in mind, support for the same trends evident from the entropy groupings can be found in the H1 layer thicknesses. H1 thicknesses reveal that as distance from the source along the margin increases, the layer thickness decreases (Fig. 1). This decreasing trend in layer thickness can be seen clearly in Fig. 2 where it has been fitted by an exponential function. The thickest H1 layers are found proximally and the entropy groupings indicate that much of this layer is composed of plume delivered sediments. All of the cores from the Labrador margin (400–1400 km) are thinner than expected from the exponential fit. This is likely because most sediment from the plume has been deposited more proximally, and this component of the total sedimentation has decreased without compensation from any other delivery mechanism. Layer thickness in cores from Orphan Basin (1400–1800 km) is well-fit by the exponential trend and reflects the relative increase in sediment delivery by ice-rafting, also evident from the entropy groupings. Layer thickness in cores from Flemish Pass (1800–2200 km) are generally higher than the exponential fit, which reflects the same increase in sediment delivery by ice-rafting as well as an increase in higher-energy sorting evident from entropy group #3 occurrences. Unlike the open slope, the bathymetry of Flemish Pass creates a sediment trap for gravity flows (Piper and Campbell, 2005).

The slope of the exponential fit of the H1 layer thickness data (Fig. 2) can be used to estimate a bulk settling velocity. This exponential fit takes the form of $y = A\ \exp^{b\ x}$ on linear axes or $y = b\ x + A_n$ on

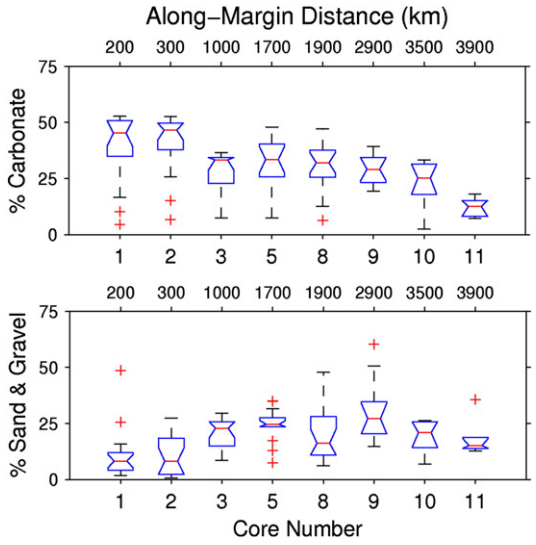

Fig. 5. Variability of carbonate and sand & gravel in along-margin cores expressed as percents by mass. The box extends from the lower quartile to upper quartile and the median is marked by a notched horizontal line. Whiskers extend to 1.5 times the interquartile range and outliers are displayed with a '+' symbol. The width of the notch in a box is calculated so that boxes whose notches do not overlap have different medians at the 5% significance level.

semilog-y axes. If the initial concentration of suspended sediment at a source is C_0, and assuming uniform particle size and first-order removal from the water column, the change in suspended sediment can be written as

$$\frac{dC}{dt} = -\lambda\, C, \tag{5}$$

which can be integrated over boundary conditions to give

$$C = C_0\, \exp^{-\lambda\, t}. \tag{6}$$

The λ variable is a decay constant with units of inverse time. Letting w_s be the diameter-dependent sinking speed of a suspended particle and h be the plume thickness, it follows that λ is proportional to w_s/h. If x is the distance along the plume trajectory and u_0 is the plume velocity (assumed constant), then $t = x/u_0$ can be substituted into Eq. (6) to give

$$C = C_0\, \exp^{-w_s\, x/h\, u_0}. \tag{7}$$

The slope of the regression, b, is equal to $w_s/h\,u$, where w_s is settling velocity, h is plume thickness, and u is plume velocity. Assuming a plume thickness of 100 m and a current speed of 50 cm/s yields a settling velocity of 0.04 mm/s for all recorded H1 layers, which is extremely low for plume sedimentation (Hill et al., 2000). This is likely the result of the dominant ice-rafting delivery of sediments for most of the region and implies that distal sites are unlikely to have significant supply of plume-delivered sediment from Hudson Strait. Considering only the H1 layer thicknesses within 1000 km of Hudson Strait, where plume sedimentation is dominant, however, yields a much steeper slope of 2.5×10^{-6} (Fig. 2). Using this slope, a settling velocity of 0.13 mm/s is calculated that is in good agreement with bulk settling velocities observed in flocculated plumes (Hill et al., 2000; Curran et al., 2002). This implies that plume-delivery of sediments is dominant within 1000 km of Hudson Strait.

The $CaCO_3$ content and sand & gravel content of each sample reflect similar trends in sediment delivery. $CaCO_3$ is delivered to the seafloor following both plume and ice-rafting transport. The sand & gravel content in H1 layers is the coarse grains whose presence in slope cores can only be explained by ice-rafting or turbidity current delivery. It follows that a change in the rate of plume delivery of sediment would change the $CaCO_3$ content of a core, a change in the rate of turbidity current delivery would change the sand & gravel content of a core, and a change in the rate of ice-rafting delivery would change both the $CaCO_3$ and sand & gravel content of a core. Ice-rafted group #2 sediments winnowed to a group #3 distribution would have elevated % sand & gravel content. Along-margin, % $CaCO_3$ decreases with a marked decline between cores 2 and 3 where plume deposition would have also decreased markedly. $CaCO_3$ levels remain relatively constant through Orphan Basin, Flemish Pass, and the SW Grand Banks (cores 5, 8, and 9) where delivery by ice-rafting is greatest. The % sand & gravel increases through the proximal region as plume delivery becomes less important, and it reaches its maxima in the Orphan Basin and Grand Banks regions. Again, this reflects the increased ice-rafting delivery likely caused by stalled icebergs and/or increased iceberg melting. Also, complex sediment dynamics and bathymetry of the region may make turbidity currents more prominent (Piper and Campbell, 2005). Shallower core sites in this region may have been subject to winnowing that produced a group #3 distribution, especially core 4 where the occurrence of a turbidity current is unreasonable. $CaCO_3$ and sand & gravel content decrease in distal cores 9–11, implying greater dilution by fine grained sediment from other sources, likely proglacial sources on the Scotian Shelf (Piper and Skene, 1998). Cross-margin, both $CaCO_3$ and sand & gravel content increase slightly and then level off or slightly decrease as the main trajectory of the advected icebergs is crossed.

Because DC is mostly derived from the Hudson Strait region (for a review of sediment provenance see Hemming, 2004), carbonate content can be used to assess the degree of dilution by non-Hudson Strait materials. Then, layer thickness can be adjusted to reflect this dilution and the normalized thicknesses can be regressed to obtain another

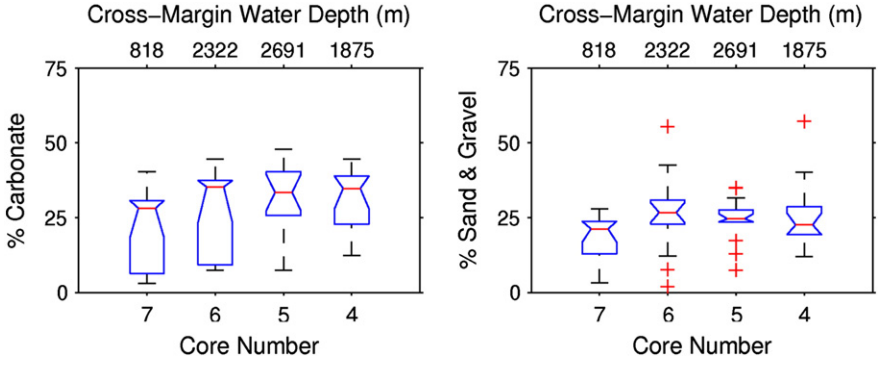

Fig. 6. Variability of carbonate and sand & gravel in cross-margin cores expressed as percents by mass. The box extends from the lower quartile to upper quartile and the median is marked by a notched horizontal line. Whiskers extend to 1.5 times the interquartile range and outliers are displayed with a '+' symbol. The width of the notch in a box is calculated so that boxes whose notches do not overlap have different medians at the 5% significance level.

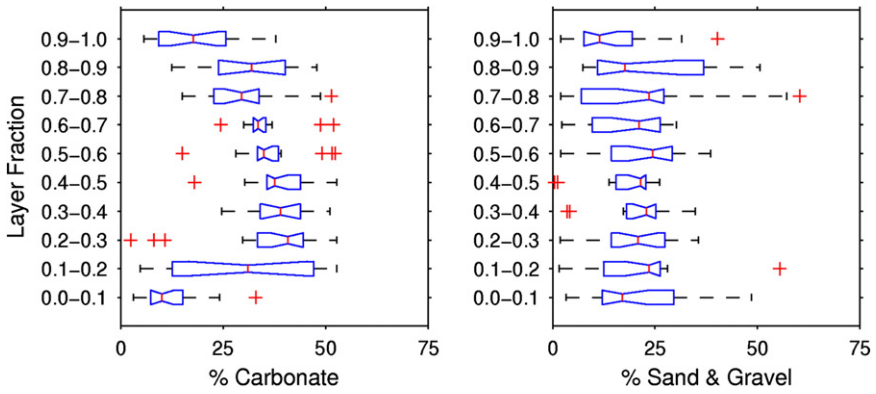

Fig. 7. Variability of carbonate and sand & gravel downcore expressed as percents by mass. The box extends from the lower quartile to upper quartile and the median is marked by a notched horizontal line. Whiskers extend to 1.5 times the interquartile range and outliers are displayed with a '+' symbol. The width of the notch in a box is calculated so that boxes whose notches do not overlap have different medians at the 5% significance level.

estimate of bulk settling velocity. The slope of the regression of eleven H1 layer thicknesses normalized to median carbonate content for each core is 1.1×10^{-6} (Fig. 8) and yields a settling velocity of 0.06 mm/s that is closer to typical bulk settling velocities than that calculated from the actual layer thicknesses. This implies that the plume signature is considerably diluted. There are lesser sources of DC in western Newfoundland and the Gulf of Saint Lawrence, but these would only affect cores 9–11 and ice-rafted gravel petrology suggests that these carbonate sources are of minor importance (Piper and DeWolfe, 2003). Thus, it appears that dilution alone cannot explain the thickness of the H1 layer in the distal region and significant delivery of sediment by ice-rafting must occur. Because of this, inferring plume processes based on properties of distal sediments is not recommended. However, the lack of plume deposited sediments distally only implies absence of plume sedimentation and does *not* imply the absence of a freshwater plume. In fact, many researchers have found evidence for extensive regions of decreased surface salinity during H events using $\delta^{18}O$ and $\delta^{13}C$ (e.g., Vidal et al., 1997; Elliot et al., 2002; Cortijo et al., 2005).

6.3. Comparison with facies interpretations

Textural interpretation of sediment dynamics during the H1 event is broadly consistent with facies interpretations based on X-radiography (Hesse and Khodabakhsh, 1998; Rashid et al., 2003a). Interpretation of sediment texture and facies within H layers from the Labrador Sea have both revealed plume fallout, ice-rafting, and turbidity current sediment delivery mechanisms, although sediment delivery by turbidity currents is sometimes divided into fast and slow mechanisms by facies analysis (i.e., Hesse and Khodabakhsh, 1998). Primary sedimentary structures have been destroyed by bioturbation in the thinner beds on the Scotian Slope. However, the delivery mechanism suggested by a particular sample DIGS distribution does not always align with the delivery mechanism suggested by interpretation of the sampled facies. It is important to note that differences in texture at grain sizes of <100 μm determined here address variability at much smaller scales than typically considered in facies analyses and cannot be distinguished visually from photographs or X-radiographs. Furthermore, winnowing of group #2 sediments by the Labrador Current may produce better sorting of the coarse fraction resulting in a group #3 distribution without a major increase in % sand & gravel. In these circumstances, groups #2 and #3 would be indistinguishable as facies in X-radiographs. Although the robustness of the application of entropy analysis to H1 sediments is limited by post-depositional re-working of sediments resulting from bioturbation and winnowing, textural analysis of H1 layers provided an objective interpretation and an additional method for investigating sediment transport during the event.

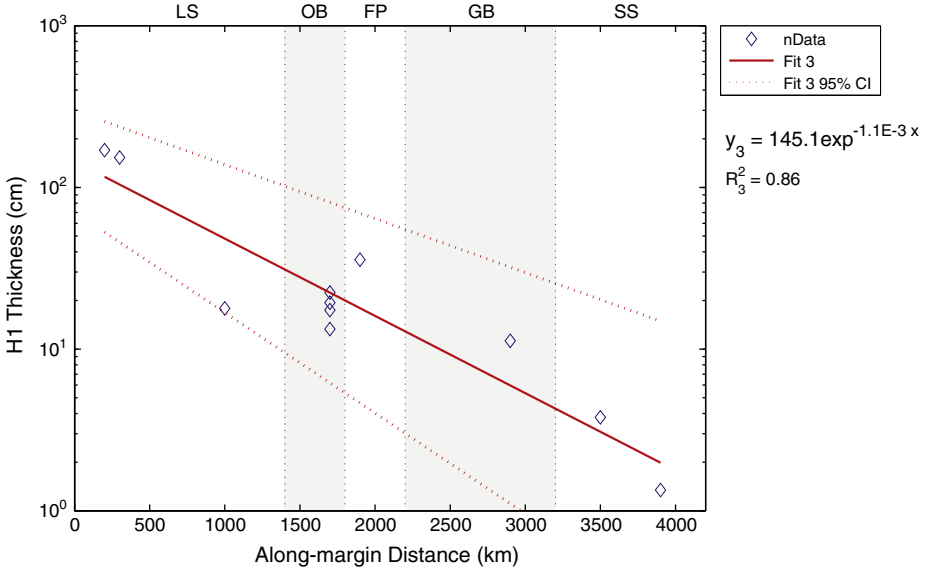

Fig. 8. H1 layer thickness (cm) by along-margin distance (km) on semilog-y axes. Layer thickness is normalized to median carbonate content for each core to account for dilution by non-Hudson Strait sources. Fit 3 is a linear regression of eleven normalized layer thicknesses and is plotted with 95% confidence intervals. The equation and R^2 value are shown. LS = Labrador Slope, OB = Orphan Basin, FP = Flemish Pass, GB = Grand Banks, SS = Scotian Slope.

7. Conclusions

Sediment deposition during H1 was dominated by plume transport within 1000 km of the Hudson Strait outlet. A mean settling velocity of 0.13 mm/s is inferred for this plume-delivered sediment. Distally, sediment transport was principally by ice-rafting. Melting of icebergs was particularly important around Orphan Basin and Flemish Pass, partly because of slowing of icebergs by bathymetric constrictions and perhaps because of the influence of warmer North Atlantic Current water. Higher-energy sorting (i.e., resulting from winnowing or turbidity currents) produces distinctive grain size distributions that are more abundant toward the end of the H1 event. Although there is no distinctive sediment plume signature in DIGS distributions from distal settings, biota provides evidence for reduced salinity in these settings. Disaggregated inorganic grain size (DIGS) analysis, coupled with entropy analysis, provides a robust means of understanding fine fraction (<100 μm) sediment dynamics in Heinrich events.

Acknowledgments

The authors would like to extend their gratitude to Francky Saint-Ange, Kate Jarrett, Tim Milligan, Jessica Carrière-Garwood, Claire Normandeau, John Newgard, and Stephanie Kienast for their contributions to this work. We also thank the reviewers of this manuscript for their suggestions. This work was funded by NSERC grants awarded to P.S. Hill and M. Kienast.

References

Andrews, J.T., 1998. Abrupt changes (Heinrich events) in late Quaternary North Atlantic marine environments: a history and review of data and concepts. Journal of Quaternary Science 13, 3–16.
Andrews, J., Tedesco, K., 1992. Detrital carbonate-rich sediments, northwestern Labrador Sea: implications for ice-sheet dynamics and iceberg rafting (Heinrich) events in the North Atlantic. Geology 20, 1087–1090.
Andrews, J.T., Tedesco, K., Briggs, W.M., Evans, L.W., 1994. Sediments, sedimentation rates, and environments, SE Baffin Bay and NW Labrador Sea 8 to 26 ka. Canadian Journal of Earth Sciences 31, 90–103.
Bard, E., Rostek, F., Turon, J.L., Gendreau, S., 2000. Hydrological impact of Heinrich events in the subtropical northeast Atlantic. Science 289, 1321–1324.
Bond, G., Heinrich, H., Broecker, W., Labeyrie, L., McManus, J., Andrews, J., Huon, S., Jantschik, R., Clasen, S., Simet, C., Tedesco, K., Klas, M., Bonani, G., Ivy, S., 1992. Evidence for massive discharges of icebergs into the North Atlantic ocean during the last glacial period. Nature 360, 245–249.
Bond, G., Broecker, W., Johnsen, S., McManus, J., Labeyrie, L., Jouzel, J., Bonani, G., 1993. Correlations between climate records from North Atlantic sediments and Greenland ice. Nature 365, 143–147.
Broecker, W.S., 1994. Massive iceberg discharges as triggers for global climate change. Nature 372, 421–424.
Broecker, W., Bond, G., Klas, M., Clark, E., McManus, J., 1992. Origin of the northern Atlantic's Heinrich events. Climate Dynamics 6, 265–273.
Cortijo, E., Duplessy, J.C., Labeyrie, L., Duprat, J., Paillard, D., 2005. Heinrich events: hydrological impact. Comptes Rendus Geoscience 337, 897–907.
Curran, K.J., Hill, P.S., Milligan, T.G., 2002. The role of particle aggregation in size-dependent deposition of drill mud. Continental Shelf Research 22, 403–414.
Curran, K.J., Hill, P.S., Schell, T.M., Milligan, T., Piper, D.J.W., 2004. Inferring the mass fraction of floc-deposited mud: application to fine-grained turbidites. Sedimentology 51, 927–944.
Dansgaard, W., Johnsen, S., Clausen, H., Dahl-Jensen, D., Gundestrup, N., Hammer, C., Hvidberg, C., Steffensen, J., Sveinbjorndottir, A., Jouzel, J., Bond, G., 1993. Evidence for general instability of past climate from a 250-kyr ice-core record. Nature 364, 218–220.
Dowdeswell, J., Maslin, M., Andrews, J., McCave, I., 1995. Iceberg production, debris rafting, and the extent and thickness of Heinrich layers (H-1, H-2) in North Atlantic sediments. Geology 23, 301–304.
Elliot, M., Labeyrie, L., Duplessy, J.C., 2002. Changes in North Atlantic deep-water formation associated with the Dansgaard–Oeschger temperature oscillations (60–10 ka). Quaternary Science Reviews 21, 1153–1165.
Grousset, F., Labeyrie, L., Sinko, J., Cremer, M., Bond, G., Duprat, J., Cortijo, E., Huon, S., 1993. Patterns of ice-rafted detritus in the glacial North Atlantic (40–55°N). Paleoceanography 8, 175–192.
Heinrich, H., 1988. Origin and consequences of cyclic ice rafting in the Northwest Atlantic Ocean during the past 130,000 years. Quaternary Research 29, 142–152.
Hemming, S.R., 2004. Heinrich events: massive Late Pleistocene detritus layers of the North Atlantic and their global climate imprint. Reviews of Geophysics 42.
Hesse, R., Khodabakhsh, S., 1998. Depositional facies of late Pleistocene Heinrich events in the Labrador Sea. Geology 26, 103–106.
Hill, P.S., Milligan, T.G., Geyer, W.R., 2000. Controls on the effective settling velocity of suspended sediment in the Eel River flood plume. Continental Shelf Research 20, 2095–2111.
Hillaire-Marcel, C., de Vernal, A., Bilodeau, G., Wu, G., 1994. Isotope stratigraphy, sedimentation rates, deep circulation, and carbonate events in the Labrador Sea during the last ~200 ka. Canadian Journal of Earth Sciences 31, 63–89.
Johnston, R.J., Semple, R.K., 1983. Classification using information statistics. Concepts and Techniques in Modern Geography No. 37. Geo Books, p. 43.
Keigwin, L.D., Lehman, S.J., 1994. Deep circulation change linked to HEINRICH event 1 and Younger Dryas in a middepth North Atlantic core. Paleoceanography 9, 185–194.
Khodri, M., Ramstein, G., Paillard, D., Duplessy, J., Kageyama, M., 2003. Modelling the climate evolution from the last interglacial to the start of the last glaciation: the role of Arctic Ocean freshwater budget. Geophysical Research Letters 30.
Kranck, K., 1980. Experiments on the significance of flocculation in the settling behaviour of fine grained sediment in still water. Canadian Journal of Earth Sciences 17, 1517–1526.
Law, B.A., Hill, P.S., Milligan, T.G., Curran, K.J., Wiberg, P.L., Wheatcroft, R.A., 2008. Size sorting of fine-grained sediments during erosion: results from western Gulf of Lions. Continental Shelf Research 28, 1935–1946.
Lebreiro, S., Moreno, J., McCave, I., Weaver, P., 1996. Evidence for Heinrich layers off Portugal (Tore Seamount: 39°N, 12°W). Marine Geology 131, 47–56.
McCave, I., Hall, I., 2006. Size sorting in marine muds: processes, pitfalls, and prospects for paleoflow-speed proxies. Geochemistry, Geophysics, Geosystems 7.
McManus, J., Francois, R., Gherardi, J.-M., Keigwin, L., Brown-Leger, S., 2004. Collapse and rapid resumption of the Atlantic meridional circulation linked to deglacial climate signals. Nature 428, 834–837.
Mikkelsen, O.A., Curran, K.J., Hill, P.S., Milligan, T.G., 2007. Entropy analysis of in situ particle size spectra. Estuarine, Coastal and Shelf Science 72, 615–625.
Milligan, T.G., Kranck, K., 1991. Electroresistance particle size analyzers. Principles, Methods, and Application of Particle Size Analysis. Cambridge University Press, pp. 109–118 (Ch. 8).
Milligan, T.G., Hill, P.S., Law, B.A., 2007. Floculation and the loss of sediment form the Po River plume. Continental Shelf Research 27, 309–321.
Orpin, A.R., Kostylev, V.E., 2006. Towards a statistically valid method of textural sea floor characterization of benthic habitats. Marine Geology 225, 209–222.
Orpin, A.R., Brunskill, G.J., Zagorskis, I., Woolfe, K.J., 2004. Patterns of mixed siliciclastic-carbonate sedimentation adjacent to a large dry-tropics river on the central Great Barrier Reef shelf, Australia. Australian Journal of Earth Sciences 51, 665–683.
Piper, D.J.W., 1988. Glaciomarine sediments on the continental slope off eastern Canada. Geoscience Canada 15, 23–28.
Piper, D.J.W., 2005. Late Cenozoic evolution of the continental margin of eastern Canada. Norwegian Journal of Geology 85, 231–244.
Piper, D.J.W., Campbell, D.C., 2005. Quaternary geology of Flemish Pass and its application to geohazard evaluation for hydrocarbon development. Geological Survey of Canada Special Paper 43, 29–43.
Piper, D.J., DeWolfe, M., 2003. Petrographic evidence from the eastern Canadian margin of shelf-crossing glaciations. Quaternary International 99–1000, 99–113.
Piper, D.J., Skene, K.I., 1998. Latest Pleistocene ice-rafting events on the Scotian Margin (eastern Canada) and their relationship to Heinrich events. Paleoceanography 13 (2), 205–214.
Rashid, H., Hesse, R., Piper, D.J.W., 2003a. Origin of unusually thick Heinrich layers in ice-proximal regions of the northwest Labrador Sea. Earth and Planetary Science Letters 208, 319–336.
Rashid, H., Hesse, R., Piper, D.J.W., 2003b. Evidence for an additional Heinrich event between H5 and H6 in the Labrador Sea. Paleoceanography 18 (4), 1077–1091.
Rea, D.K., 1994. The paleoclimatic record provided by Eolian deposition in the deep sea: the geologic history of wind. Reviews of Geophysics 32, 159–195.
Shannon, C.E., 1948. A mathematical theory of communication. The Bell System Technical Journal 27 (379–423), 623–656.
Sheldon, R.W., Prakash, A., Sutcliffe Jr., W.H., 1972. The size distribution of particles in the ocean. Limnology and Oceanography 17, 327–339.
Stewart, L.K., Kostylev, V.E., Orpin, A.R., 2009. Windows-based software for optimising entropy-based groupings of textural data. Computers & Geosciences 35, 1552–1556.
Stocker, T.F., 2000. Past and future reorganizations in the climate system. Quaternary Science Reviews 19, 301–319.
Talley, L.D., McCartney, M.S., 1982. Distribution and circulation of Labrador Sea Water. Journal of Physical Oceanography 12, 1189–1205.
Vidal, L., Labeyrie, L., Cortijo, E., Arnold, M., Duplessy, J.C., Michel, E., Becque, S., van Weering, T.C.E., 1997. Evidence for changes in the North Atlantic Deep Water linked to meltwater surges during the Heinrich events. Earth and Planetary Science Letters 146, 13–27.
Voelker, A.H.L., 2001. Global distribution of centennial-scale records for Marine Isotope Stage (MIS) 3: a database. Quaternary Science Reviews 21, 1185–1212.
Wang, D., Hesse, R., 1996. Continental slope sedimentation adjacent to an ice-margin. II. Glaciomarine depositional facies on Labrador Slope and glacial cycles. Marine Geology 135, 65–96.
Woolfe, K.J., Michibayashi, K., 1995. "Basic" entropy grouping of laser-derived grain-size data: an example from the Great Barrier Reef. Computers and Geosciences 21, 447–462.